

## Full Length Article

Effect of defects on adsorption characteristics of AlN monolayer towards SO<sub>2</sub> and NO<sub>2</sub>: Ab initio exposureTianhong Ouyang<sup>a</sup>, Zhao Qian<sup>a,\*</sup>, Xiaopeng Hao<sup>a</sup>, Rajeev Ahuja<sup>b</sup>, Xiangfa Liu<sup>a</sup><sup>a</sup> Key Laboratory for Liquid-Solid Structural Evolution & Processing of Materials (Ministry of Education), Suzhou Institute of Shandong University, State Key Lab of Crystal Materials, Shandong University, China<sup>b</sup> Condensed Matter Theory Group, Department of Physics and Astronomy, Ångström Laboratory, Uppsala University, Sweden

## ARTICLE INFO

## Keywords:

AlN monolayer  
Vacancy defects  
Adsorption  
Electronic structure  
DFT  
First-principles

## ABSTRACT

Density functional theory (DFT) calculations have been employed to explore the adsorption properties of pristine and vacancy-defective AlN monolayer towards SO<sub>2</sub> and NO<sub>2</sub> in terms of their adsorption energies and electronic structures. The calculations with van der Waals effect are performed to study the binding mechanism of pristine and vacancy-defective AlN nanosheet with SO<sub>2</sub> and NO<sub>2</sub>. Three types of vacancy defects are considered including Al-monovacancy, N-monovacancy and divacancy. The adsorption energies of vacancy-defective AlN monolayer towards SO<sub>2</sub> and NO<sub>2</sub> are found to be much higher than that of pristine nanosheet. The equilibrium adsorption sites and configurations of the gas molecules on AlN nanosheets are determined. The Bader charge transfer analysis reveals that a considerable amount of charge is transferred from the vacancy-defective AlN nanosheets to the gases leading to the increase of adsorption energies. The results of difference charge densities, band structures, electronic density of states and work function further give insight into adsorption energies. The dramatic changes of electronic band structures after gas interaction suggest the excellent adsorption properties of vacancy-defective AlN monolayer towards SO<sub>2</sub> and NO<sub>2</sub>.

## 1. Introduction

With rapid progress in synthesis and characterization of two-dimensional materials such as graphene [1], transition metal dichalcogenides (TMDs) [2], silicene [3], germanene [4], and phosphorene [5], they are becoming hopeful candidates in a wide-ranged application due to their unusual properties. Gas detection is one of the applications developed for a few decades with more efficient gas detectors being exploited [6,7]. Two-dimensional materials are usually good candidates for gas detection or filtration on account of their high surface-to-volume ratios so that the gas molecules can be exposed to a large surface area. The adsorption properties of two-dimensional graphene-based material have been investigated early both theoretically [8–11] and experimentally [12,13]. These studies indicate that by the charge transfer between gas molecules and nanosheets, the electron conductivity of the substrates can be changed after gas adsorption. While, the lack of band gap in pristine graphene actuates some researchers to find more 2D materials that possess more considerable performance of gas detection or filtration. Therefore, the adsorption properties of many 2D materials such as silicene [14], phosphorene [15], monolayer BN [16] and MoS<sub>2</sub> [17] towards different gases have been reported in recent years.

The aluminium nitride (AlN) nanosheet is another kind of 2D material which has a wide indirect band gap of 2.93 eV [18,19]. Zhang et al. had successfully fabricated the single crystalline AlN nanosheets on Si substrates by a vapor-phase transport method using Al powder and ammonia as the source materials, which are uniform and smooth [20]. The structural, electronic and magnetic properties of pure and decorated AlN nanosheets were investigated through first-principles computations [21–23]. The pure material has good performance of gas detection towards formaldehyde [24], SO<sub>2</sub> [25] and NO<sub>2</sub> [26]. Our previous work shows that both the C-doping and the N-vacancy defect improve the CO adsorption energies of AlN nanosheet [27].

Although some pure 2D-materials exhibit good adsorption properties, more efficient gas detectors or filters can be further developed by doping/decorating with hetero-atoms or introducing vacancy defects based on the pure materials. For example, Zhang et al. investigated the interactions between graphene-based materials including B-, N-doped and defective substrates and small gas molecules such as CO, NO, NO<sub>2</sub> and NH<sub>3</sub> [28]. The results show that the defective graphene has the highest adsorption energy with CO, NO and NO<sub>2</sub> molecules, while the B-doped graphene gives the tightest binding with NH<sub>3</sub>, which implies that the sensitivity of graphene-based chemical gas detectors could be

\* Corresponding author.

E-mail address: [qianzhao@sdu.edu.cn](mailto:qianzhao@sdu.edu.cn) (Z. Qian).<https://doi.org/10.1016/j.apsusc.2018.08.073>

Received 17 May 2018; Received in revised form 4 June 2018; Accepted 6 August 2018

Available online 07 August 2018

0169-4332/ © 2018 Elsevier B.V. All rights reserved.

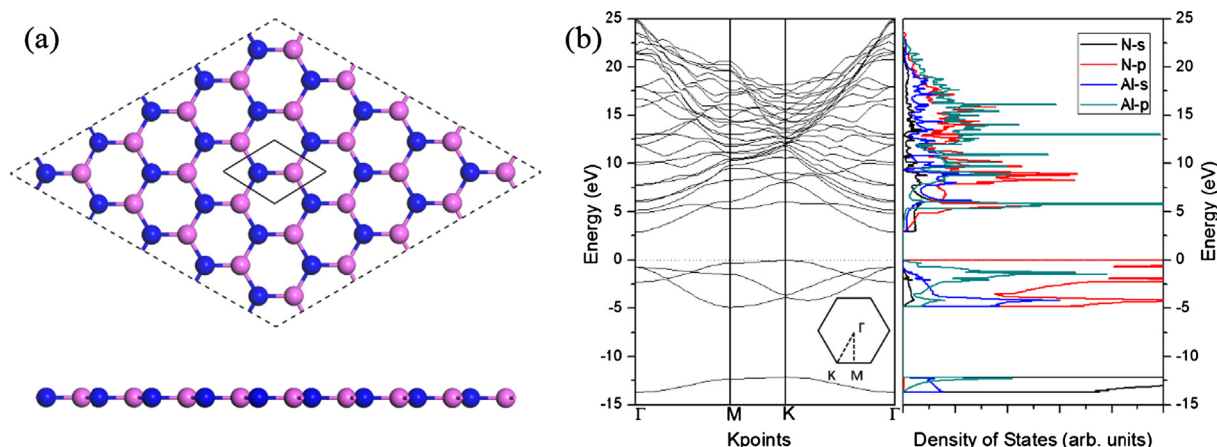


**Fig. 1.** (a) Top and side views of pristine AlN monolayer. The solid and dashed hexagons in the top view show the primitive cell and the  $5 \times 5$  supercell, respectively. (b) The electronic band structure and projected density of states (PDOS) of pristine AlN nanosheet. The Fermi energy is set to zero. The inset shows the first Brillouin zone and the high-symmetry points in it. Blue and pink balls represent N and Al atoms, respectively.

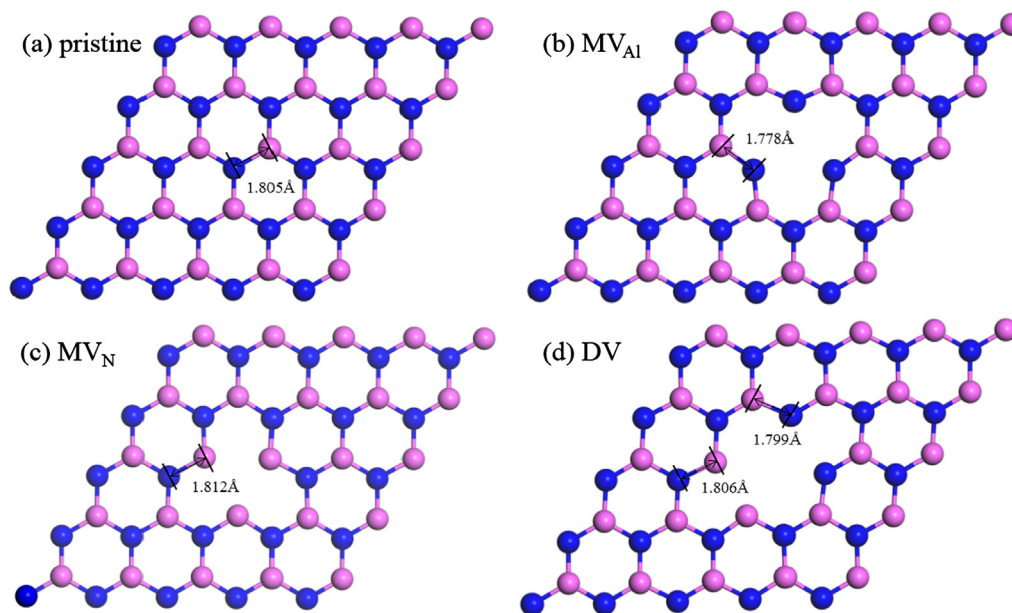


**Fig. 2.** Top view of optimized structures of (a) pristine, (b) Al-monovacancy, (c) N-monovacancy, and (d) divacancy defective AlN nanosheets.

drastically improved by introducing the appropriate dopants or defects. Hussain et al. investigated the structural, electronic, and adsorption properties of pure, defective and substituted silicene monolayers, which reveals that the vacancy defect in silicene drastically changes the electronic properties and improves the binding of exposed  $\text{CO}_2$ ,  $\text{H}_2\text{S}$  and  $\text{SO}_2$  gas molecules signally [29]. The binding mechanism of pristine and defective phosphorene towards the toxic gases  $\text{PH}_3$  and  $\text{AsH}_3$  has been explored showing that the introduction of defects such as monovacancies and divacancies in the phosphorene sheet can help to improve the adsorption energies [30]. Ma et al. investigated the interactions between the  $\text{MoS}_2$  monolayer with the S vacancies and CO, NO and  $\text{NO}_2$  molecules, which reveals that the S vacancy can be repaired by the adsorption of CO, NO and  $\text{NO}_2$  molecules at room temperature [31].

However, for the AlN nanosheet system, the effect of vacancy defects on its adsorption properties has not been exposed systematically. In this study, we explore the adsorption properties of AlN monolayer with two types of monovacancy or divacancies in the presence of  $\text{SO}_2$  and  $\text{NO}_2$ . Sulfur dioxide ( $\text{SO}_2$ ) is a highly hazardous gas and can damage the human respiratory system through inhalation [32], which is also one source of pollutive haze or smog [33]. The nitrogen dioxide ( $\text{NO}_2$ ) is generally found in vehicle exhaust and is also known as a toxic

gas harmful to the respiratory system [34]. This theoretical investigation based on first-principles computations would be essential to guide the experimentalists and supply more underlying electronic origin for the design of vacancy defective or functionalized AlN nanosheets as gas detection or filtration materials, which will also be meaningful for developing more efficient two-dimensional gas absorbents in the near future.

## 2. Theoretical methods

All of the first-principles calculations presented in this work were performed within the framework of Density Functional Theory (DFT), as implemented in Vienna Ab initio Simulation Package (VASP) [35–39]. The projector augmented wave (PAW) [40] potentials were used to describe the electron-ion interactions. The generalized gradient approximation (GGA) functional in the form of Perdew–Burke–Ernzerhof (PBE) [41] was used to treat the exchange correlation energy. The DFT-D2 method of Grimme [42] to describe correctly the van der Waals interactions was considered to calculate the weak and long-range interactions. The AlN nanosheet was modelled by  $(5 \times 5 \times 1)$  supercell including 25 Al atoms and 25 N atoms. To minimize the interaction

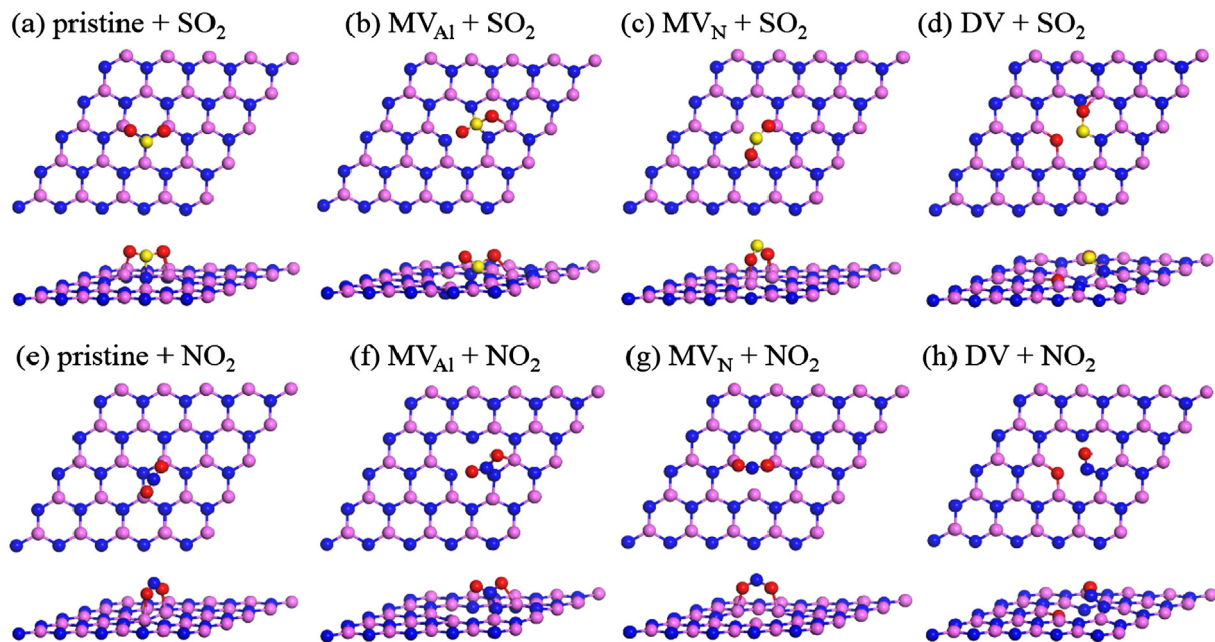


**Fig. 3.** Top and side views of stable configurations of a gas molecule of  $\text{SO}_2$  or  $\text{NO}_2$  on (a, e) pristine, (b, f) Al-monovacancy, (c, g) N-monovacancy, (d, h) divacancy defective AlN nanosheets. Blue, pink, red and yellow balls represent N, Al, O, and S atoms, respectively. (For interpretation of the references to color in this figure legend, the reader is referred to the web version of this article.)

**Table 1**

Adsorption Energies ( $E_{\text{ad}}$ , eV), distances between gas molecule and nanosheets ( $d$ , Å), band gaps ( $E_g$ , eV), work functions ( $\Phi$ , eV) and charge transfer (CT, e) of the lowest-energy configurations of  $\text{SO}_2$  or  $\text{NO}_2$  gas molecule on pristine,  $\text{MV}_{\text{Al}}$ ,  $\text{MV}_{\text{N}}$  and DV AlN nanosheets. Distances between gas molecule and nanosheets are defined as the nearest distance between the atom in gas molecule and the atom in AlN nanosheets. Positive CT values represent electron transfer from the AlN nanosheets to the gas molecule.

|   | $E_{\text{ad}}$ (eV) | $d$ (Å) | $E_g$ (eV) | $\Phi$ (eV) | CT (e) |
|---|----------------------|---------|------------|-------------|--------|
| Pristine                                | –                    | –       | 2.93       | 5.26        | –      |
| $\text{MV}_{\text{Al}}$                 | –                    | –       | 2.70       | 5.15        | –      |
| $\text{MV}_{\text{N}}$                  | –                    | –       | 2.94       | 4.71        | –      |
| DV                                      | –                    | –       | 2.70       | 5.05        | –      |
| Pristine + $\text{SO}_2$                | –5.26                | 1.72    | 2.98       | 5.42        | 0.55   |
| $\text{MV}_{\text{Al}}$ + $\text{SO}_2$ | –9.50                | 1.61    | 3.05       | 5.21        | –0.48  |
| $\text{MV}_{\text{N}}$ + $\text{SO}_2$  | –6.88                | 1.88    | 3.01       | 4.40        | 0.99   |
| DV + $\text{SO}_2$                      | –9.95                | 1.62    | 2.15       | 4.41        | 1.25   |
| Pristine + $\text{NO}_2$                | –4.61                | 2.02    | 3.01       | 5.49        | 0.81   |
| $\text{MV}_{\text{Al}}$ + $\text{NO}_2$ | –7.71                | 1.31    | 2.73       | 5.31        | 0.64   |
| $\text{MV}_{\text{N}}$ + $\text{NO}_2$  | –8.32                | 1.93    | 2.94       | 5.26        | 0.97   |
| DV + $\text{NO}_2$                      | –11.00               | 1.33    | 2.14       | 4.61        | 1.83   |

between the periodic adjacent layers, the vacuum space of 20 Å was set along the  $z$  direction. The Brillouin zone integrations were sampled using the Monkhorst–Pack grid of  $5 \times 5 \times 1$  (in the stage of geometry optimization) and  $15 \times 15 \times 1$  (in the stage of density of states calculations) [43]. An energy cutoff of 520 eV was chosen for the plane wave basis set. The optimized structure was gained using the conjugate gradient algorithm to relax all ionic positions until the tolerance in the total energy was lower than 0.0001 eV between two ionic steps. The charge profile has been performed by using Bader analysis [44]. The adsorption energies of gas molecules on the surface of AlN nanosheets were evaluated in the following equation:

$$E_{\text{ad}} = E_{\text{AlN+gas}} - E_{\text{AlN}} - E_{\text{gas}} \quad (1)$$

where  $E_{\text{ad}}$ ,  $E_{\text{AlN+gas}}$ ,  $E_{\text{AlN}}$  and  $E_{\text{gas}}$  are the adsorption energy, the total energies of optimized AlN nanosheets with adsorbed gas molecules, bare AlN nanosheet and isolated  $\text{SO}_2$  (or  $\text{NO}_2$ ) respectively. Therefore, the negative value of  $E_{\text{ad}}$  indicates the thermodynamic stability of the

adsorption systems. In addition, the formation energies of the vacancy defects have been resolved by the following formula:

$$E_f = E_{\text{defective}} + E_{\text{atom(s)}} - E_{\text{pristine}} \quad (2)$$

where  $E_f$ ,  $E_{\text{defective}}$ ,  $E_{\text{pristine}}$  and  $E_{\text{atom(s)}}$  stand for the formation energies, the total energies of optimized vacancy-defective AlN nanosheets, pristine AlN nanosheet and Al (or N) atoms removed from the sheet, respectively. Therefore, the value of  $E_f$  implies the difficulty of formation of vacancy defects.

### 3. Results and discussion

First of all, the geometric structure of pristine AlN monolayer has been optimized as shown in Fig. 1, which exhibits a flat graphene-like honeycomb structure. The calculated lattice constant of 3.12 Å and Al–N bond length of 1.805 Å are in good agreement with the previous investigations [18]. There is an indirect band gap of 2.93 eV from K to  $\Gamma$  point exhibiting in the band structure of AlN sheet, which is smaller than that of the bulk structure [45]. From the projected density of states (PDOS), it can be seen that the valance-band maximum is dominated by N-p states and that the peak of Al-p states resonating with N-p states indicates that the binding between Al and N atoms is formed through the overlap of Al-p and N-p orbitals. To study the gas adsorption properties of vacancy-defective AlN nanosheets, firstly the geometric structures of three types of AlN nanosheets with Al-monovacancy ( $\text{MV}_{\text{Al}}$ ), N-monovacancy ( $\text{MV}_{\text{N}}$ ), and divacancy (DV) have been calculated as plotted in Fig. 2. The formation energies of  $\text{MV}_{\text{Al}}$ ,  $\text{MV}_{\text{N}}$  and DV are 14.23, 10.27 and 18.76 eV for the supercell systems respectively. The three N atoms near the vacancy in  $\text{MV}_{\text{Al}}$ -AlN nanosheet scatter from the centre of vacancy, presenting the shortening of adjacent Al–N bonds. In  $\text{MV}_{\text{N}}$ -AlN nanosheet, three Al atoms near the vacancy assemble towards the centre of defect. Both of the phenomena appear in DV-AlN nanosheet.

$\text{SO}_2$  and  $\text{NO}_2$  are two kinds of hazardous gases which have some similar characteristics such as being harmful to human's respiratory system and causing the formation of acid rain and aggravating haze. Their molecular morphologies are also similar containing two oxygen atoms and a non-metallic atom that are connected with two bonds



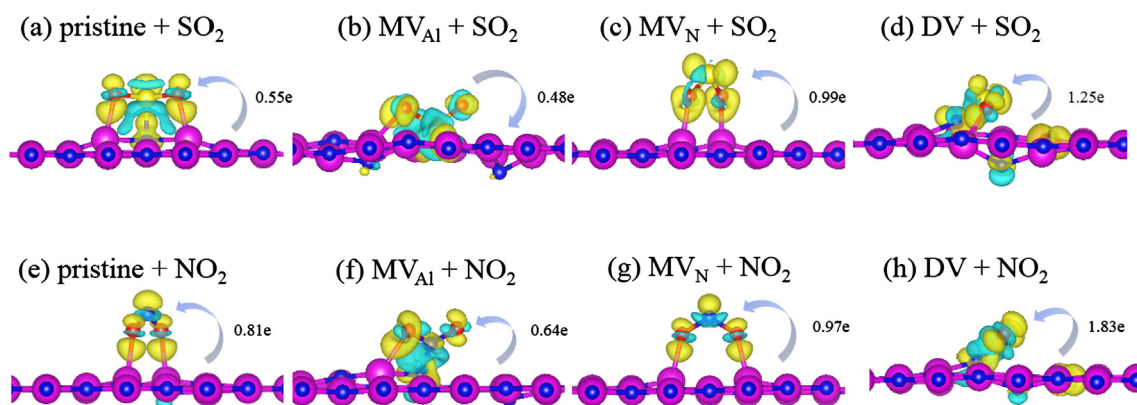


**Fig. 4.** Difference charge density plots of (a, e) pristine, (b, f)  $\text{MV}_{\text{Al}}$ , (c, g)  $\text{MV}_{\text{N}}$ , (d, h) DV-AlN nanosheets with  $\text{SO}_2$  or  $\text{NO}_2$  gas molecule (yellow, accumulation; cyan, depletion). The isovalue of charge density is  $0.01 \text{ e}/\text{\AA}^3$ . The amount and direction of charge transfer are indicated for each system by arrows. (For interpretation of the references to color in this figure legend, the reader is referred to the web version of this article.)

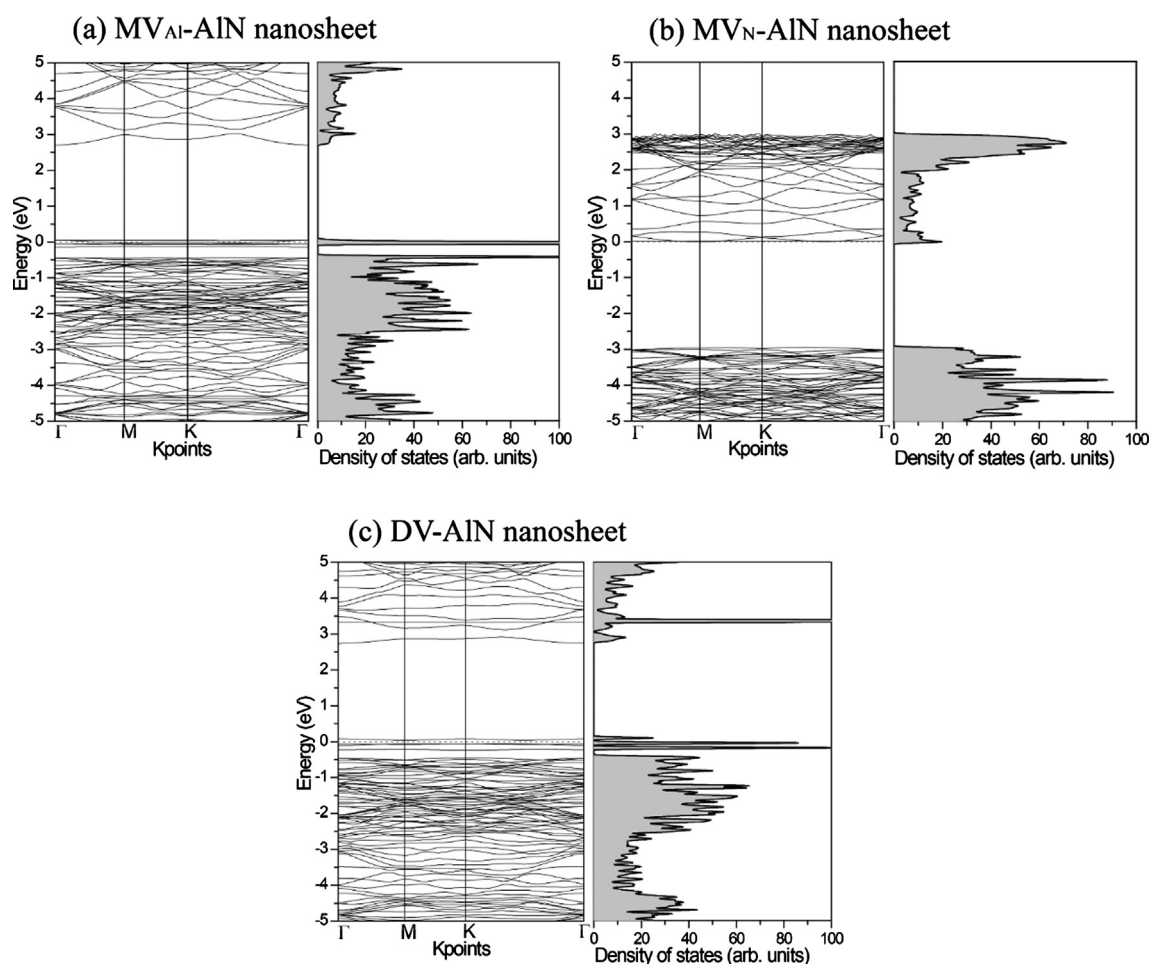


**Fig. 5.** Band structures and density of states (DOS) of bare (a)  $\text{MV}_{\text{Al}}$ , (b)  $\text{MV}_{\text{N}}$  and (c) DV-AlN nanosheets. Fermi energy is set to zero.

shaping into boomerang. With fossil fuel burning in factories and engines of vehicles,  $\text{SO}_2$  and  $\text{NO}_2$  are emitted into atmosphere as main air pollutants. Therefore, it is significant to monitor and treat them. In this fundamental research, to understand the details of  $\text{SO}_2$  and  $\text{NO}_2$  adsorption on AlN nanosheets system, different sites on all AlN nanosheets have been considered to explore the most stable adsorption configurations including the S (or N) atom below two O atoms and above the sheet, one S–O (N–O) bond paralleling to the sheet, two O atoms below S (or N) atom and above the sheet, and the plane of O–S–O (O–N–O) bond angle paralleling to the sheet. The procedure of finding the most

stable configuration has been repeated in all pristine and defective AlN systems.

For  $\text{SO}_2$ , it is found that the molecule prefers to interact with the pristine AlN nanosheet by the  $\text{SO}_2$  paralleling to the surface of the sheet with O and S atoms binding to Al and N atoms, respectively shown in Fig. 3(a). The adsorption energy and the binding distance of  $\text{SO}_2$  adsorbed on pristine AlN nanosheet are  $-5.26 \text{ eV}$  and  $1.72 \text{ \AA}$ , respectively in Table 1. Full structural relaxation shows the stretching in S–O bond from  $1.447 \text{ \AA}$  to  $1.548 \text{ \AA}$  and the reduction in O–S–O angle from  $119.171^\circ$  to  $101.323^\circ$ . In the system of  $\text{SO}_2$  adsorption on  $\text{MV}_{\text{Al}}$ -AlN

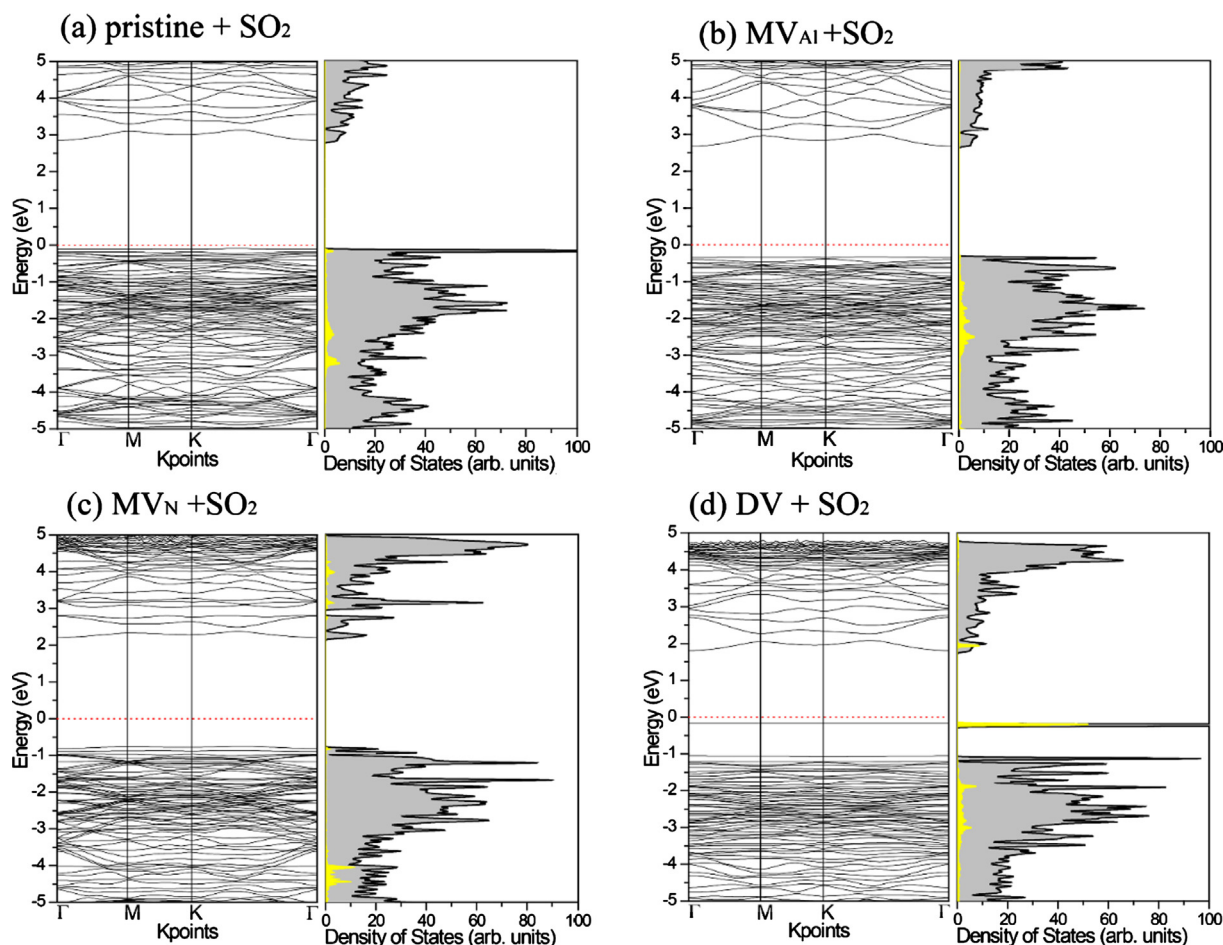


**Fig. 6.** Band structures and density of states (DOS) of  $\text{SO}_2$  molecule adsorbed on (a) pristine, (b)  $\text{MV}_{\text{Al}}$ , (c)  $\text{MV}_{\text{N}}$  and (d) DV-AlN nanosheets. The black shaded curves represent the total DOS, while the yellow colors stand for the projection of DOS onto  $\text{SO}_2$  molecule. Fermi energy is set to zero. (For interpretation of the references to color in this figure legend, the reader is referred to the web version of this article.)

nanosheet, the S atom bonds with two N atoms at the edge of the vacancy and the O atom bonds with Al atom (Fig. 3b). The adsorption energy and the binding distance of  $\text{SO}_2$  adsorbing on  $\text{MV}_{\text{Al}}$ -AlN nanosheet are  $-9.50$  eV and  $1.61$  Å, respectively. The two S–O bonds elongate to  $1.451$  Å and  $1.935$  Å and the O–S–O angle decreases to  $115.825^\circ$ . The  $\text{SO}_2$  molecule is adsorbed on  $\text{MV}_{\text{N}}$ -AlN nanosheet by the S atom away from the sheet and O atoms binding with Al atoms. This configuration has a binding energy of  $-6.88$  eV and presents a corresponding surface–adsorbate distance of  $1.88$  Å. As seen in Fig. 3(c), the  $\text{SO}_2$  molecule rearranges its geometry with elongation of one of the S–O bond angles to  $1.548$  Å and another to  $1.546$  Å from the initial value of  $1.447$  Å. The O–S–O angle also changes and reduces considerably from  $119.171^\circ$  to  $106.154^\circ$ . The lowest-energy configuration for the case of  $\text{SO}_2$  adsorbed on DV-AlN nanosheet has been shown in Fig. 3(d) with adsorption energy of  $-9.95$  eV and adsorption distance of  $1.62$  Å. Noteworthy, the  $\text{SO}_2$  molecule has been decomposed through adsorption with one of the O atoms separated and the other remaining in connection with S atom with the bond length of  $1.528$  Å larger than the value of  $1.447$  Å as a free molecule. From the data listed in Table 1, it is obvious that the adsorption energies of  $\text{SO}_2$  on vacancy-defective (including  $\text{MV}_{\text{Al}}$ ,  $\text{MV}_{\text{N}}$  and DV) AlN nanosheets are larger than that of  $\text{SO}_2$  adsorbed on pristine AlN system.

For  $\text{NO}_2$ , the pristine AlN nanosheet exhibits affinity towards it with an adsorption energy of  $-4.61$  eV and binding distance of  $2.02$  Å. But unlike the configuration of  $\text{SO}_2$  adsorbed on pristine AlN nanosheet, the N atom in  $\text{NO}_2$  molecule is away from the plane of the sheet with repelling the N atom in the sheet to “stick out” from the sheet in the negative direction (Fig. 3e). The two N–O bond lengths of  $\text{NO}_2$

molecule are altered to  $1.271$  Å and  $1.267$  Å from  $1.212$  Å and the O–N–O bond angle is reduced from  $132.915^\circ$  to  $118.629^\circ$ . A different configuration of adsorption appears in system of  $\text{NO}_2$  adsorbed on  $\text{MV}_{\text{Al}}$ -AlN nanosheet, which shows that the N atom in  $\text{NO}_2$  molecule is jointed with the N atom in the sheet at the edge of vacancy as imaged in Fig. 3(f). The adsorption energy of  $\text{NO}_2$  on  $\text{MV}_{\text{Al}}$ -AlN nanosheet is  $-7.71$  eV with a binding distance of  $1.31$  Å. Two O–N bonds are stretched to  $1.288$  Å and  $1.340$  Å respectively and the O–N–O bond angle is enlarged to  $121.444^\circ$ . In the system of  $\text{MV}_{\text{N}}$ -AlN nanosheet, one  $\text{NO}_2$  molecule adsorbed on the sheet has made the total energy of system changed for  $8.32$  eV. Just like the  $\text{NO}_2$  adsorbed on pristine AlN nanosheet, the N atom in  $\text{NO}_2$  molecule keeps away from the plane of the sheet. The value of binding distance is  $1.93$  Å. A deformation happens in  $\text{NO}_2$  molecule with two N–O bonds lengths changing to  $1.281$  Å and  $1.282$  Å and the O–N–O angle to  $115.903^\circ$ . After adsorbed on DV-AlN nanosheet, the  $\text{NO}_2$  molecule has one N–O bond splitted and the other remaining in linking as shown in Fig. 3(h), which leads to an improvement in adsorption energy of  $-11.00$  eV. The decomposed molecule binds with the sheet with a distance of  $1.33$  Å and the length of the rest N–O bond is  $1.236$  Å. All the values of adsorption energies and binding distances have been listed in Table 1, which indicates that the vacancy defects can drastically improve the adsorption energies of  $\text{NO}_2$  on AlN nanosheets.

To understand the mechanism of  $\text{SO}_2$  and  $\text{NO}_2$  adsorption on AlN nanosheets, the isosurfaces of the difference charge densities of various systems and the Bader charge transfer profiles have been plotted in Fig. 4. The charge is considerably polarized as accumulating to the bonds between gas molecule and the nanosheets, which indicates the

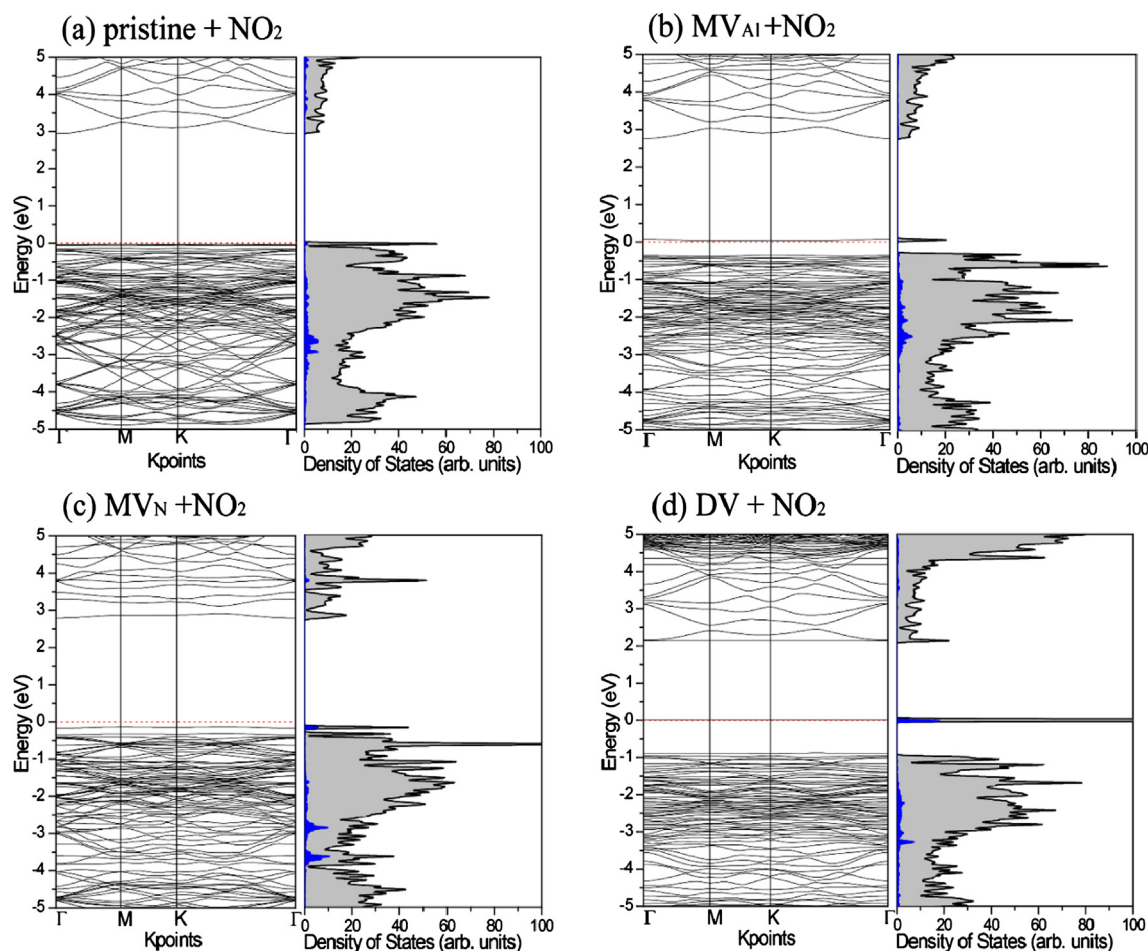


**Fig. 7.** Band structures and density of states (DOS) of  $\text{NO}_2$  molecule adsorbed on (a) pristine, (b)  $\text{MV}_{\text{Al}}$ -, (c)  $\text{MV}_{\text{N}}$ - and (d)  $\text{DV-AlN}$  nanosheets. The black shaded curves represent the total DOS, while the blue colors stand for the projection of DOS onto  $\text{NO}_2$  molecule. Fermi energy is set to zero. (For interpretation of the references to color in this figure legend, the reader is referred to the web version of this article.)

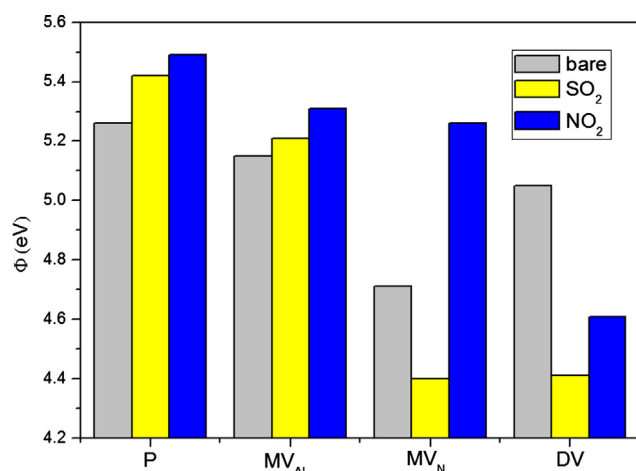


**Fig. 8.** Work functions of pristine,  $\text{MV}_{\text{Al}}$ -,  $\text{MV}_{\text{N}}$ - and  $\text{DV-AlN}$  nanosheets adsorbed by  $\text{SO}_2$  or  $\text{NO}_2$  gas molecule.

chemisorption between gas molecule and the sheets. Except the system of  $\text{SO}_2$  adsorbed on  $\text{MV}_{\text{Al}}$ -AlN nanosheet, the directions of Bader charge transfer are all from the nanosheets to the gas molecule. It can be seen that the Bader charge transfer can be dramatically magnified by introducing divacancy defects into the pristine AlN nanosheet in the presence of  $\text{SO}_2$  or  $\text{NO}_2$ .

The band structure and density of states (DOS) of three types of AlN

nanosheets with vacancy defects are shown in Fig. 5. Compared with the band structure of pristine AlN nanosheet shown in Fig. 1(b), some localized flat bands appear above the valance bands top of the  $\text{MV}_{\text{Al}}$ -AlN nanosheet caused by unpaired electrons offered by N atom near the vacancy, which implies that it is a deep-level defect. The Fermi level of  $\text{MV}_{\text{N}}$ -AlN nanosheet emerges at the conduction band bottom, which indicates that the AlN nanosheet with N-vacancy in high concentration is n-type semiconductor because the Al atoms at the edge of vacancy offer more free electrons. For DV-AlN nanosheet, three flat bands are localized approaching the Fermi level, which are offered by two N atoms near the vacancy. And the appearance of the peak in conduction band is attributed to the unpaired electrons offered by two Al atoms at the edge of vacancy.

After investigating the band structures and DOS of different bare AlN nanosheets, we have also studied the band structures and DOS of  $\text{SO}_2$  and  $\text{NO}_2$  adsorbed on four types of AlN nanosheets. For  $\text{SO}_2$  (Fig. 6), the projection of DOS onto  $\text{SO}_2$  molecule (shown in yellow) exhibits some peaks near the Fermi level especially for the  $\text{SO}_2$  adsorbed on DV-AlN nanosheet, which implies strong interactions between  $\text{SO}_2$  molecule and the substrate. In the system of  $\text{SO}_2$  adsorbed on DV-AlN nanosheet, a flat band at the Fermi level suggests that some electrons are confined in a localized state. In comparison to  $\text{SO}_2$ , there are more localized states in the systems of  $\text{NO}_2$  adsorbed on four types of AlN nanosheets (Fig. 7). The localized states remain deep-level doping or defects that have many functions such as effective compound center and compensated impurity. All localized states that have abilities of adsorbing and releasing electrons can dramatically change the



electroconductivity of the sheets, which is a paramount property for gas detection. From Table 1, it can be seen that after SO<sub>2</sub> or NO<sub>2</sub> adsorbed on pristine, MV<sub>Al</sub>- and MV<sub>N</sub>-AlN nanosheets, the band gaps of these systems all increase.

To further understand the effect of the adsorbed molecule on different AlN nanosheets, the work functions  $\Phi$  of all adsorbed systems and the bare sheets have been calculated shown in Fig. 8. The work function is the minimum amount of energy required to remove an electron from the Fermi level to infinity, which can be evaluated as:

$$\Phi = V(\infty) - E_F \quad (3)$$

where  $\Phi$ ,  $V(\infty)$ , and  $E_F$  are the work function, electrostatic potential at the vacuum level and the Fermi energy of the AlN nanosheets, respectively. The work function of bare pristine AlN nanosheet is 5.26 eV. By introducing MV<sub>Al</sub>, MV<sub>N</sub> and DV defects, the work function decreases to 5.15, 4.17 and 5.05 eV, respectively. In the system of pristine AlN nanosheet, the work function is augmented after SO<sub>2</sub> or NO<sub>2</sub> adsorption, which indicates that the electrons are restricted more tightly to the sheet. The same situation appears in the system of MV<sub>Al</sub>-AlN nanosheets. In the system of MV<sub>N</sub>-AlN nanosheet, the changes of work functions between SO<sub>2</sub> and NO<sub>2</sub> adsorption on the sheet are on the contrary. The work function of the system of SO<sub>2</sub> gas molecule adsorbed on MV<sub>N</sub>-AlN nanosheet is lower than that of bare MV<sub>N</sub>-AlN nanosheet, while in presence of NO<sub>2</sub> gas molecule the work function increases impressively. When SO<sub>2</sub> or NO<sub>2</sub> molecule is adsorbed on DV-AlN nanosheet, a reduction of work function occurs.

#### 4. Summary and outlook

The present study reports a systematic analysis of the adsorption properties of pristine and vacancy-defective AlN nanosheets exposed to the hazardous SO<sub>2</sub> or NO<sub>2</sub> gas molecule from the perspective of atomic and electronic structures. The results based on DFT calculation are analyzed in terms of adsorption energy, Bader charge transfer, difference charge density, band structure, electronic density of states and work functions. It is found that the Al-monovacancy (MV<sub>Al</sub>), N-monovacancy (MV<sub>N</sub>), and divacancy (DV) defects in AlN nanosheet change the corresponding electronic properties and the gas adsorption characteristics remarkably. The adsorption energies of SO<sub>2</sub> and NO<sub>2</sub> adsorbed on MV<sub>Al</sub>-, MV<sub>N</sub>- and DV-AlN nanosheets are much higher than that of SO<sub>2</sub> and NO<sub>2</sub> adsorbed on pristine AlN nanosheet. In the case of DV-AlN nanosheet, SO<sub>2</sub> and NO<sub>2</sub> gas molecule can even be decomposed through adsorption. The difference charge density, Bader charge transfer, band structure and electronic density of states imply that there are strong interactions between SO<sub>2</sub>/NO<sub>2</sub> gas molecule and all types of defective AlN nanosheets that manifest the process of chemisorption. The dramatical changes of band structures induced by gas interaction suggest the potential of vacancy-defective AlN nanosheets as promising candidates for effective SO<sub>2</sub> and NO<sub>2</sub> adsorption or filtration applications.

#### Acknowledgements

We would like to thank the supports from the Natural Science Foundation of China (51801113), the Natural Science Foundation of Shandong Province (ZR2018MEM001), Jiangsu Province Science Foundation for Youths (BK20160370) and the Shandong Postdoctoral Innovation Program (201602019). The Natural Science Foundations of China (51731007, 51571133, 51572153) are also acknowledged. R.A. thanks Swedish Research Council (VR) and Swedish Supercomputer facility (SNIC) for support. Some scientific calculations in this paper have been done on the HPC Cloud Platform of Shandong University.

#### References

- [1] K.S. Novoselov, A.K. Geim, S.V. Morozov, D. Jiang, Y. Zhang, S.V. Dubonos, I.V. Grigorieva, A.A. Firsov, Electric field effect in atomically thin carbon films, *Science* 306 (2004) 666–669.
- [2] M. Chhowalla, H.S. Shin, G. Eda, L.J. Li, K.P. Loh, H. Zhang, The chemistry of two-dimensional layered transition metal dichalcogenide nanosheets, *Nat. Chem.* 5 (2013) 263–275.
- [3] P. Vogt, P. De Padova, C. Quaresima, J. Avila, E. Frantzeskakis, M.C. Asensio, A. Resta, B. Ealet, G. Le Lay, Silicene: compelling experimental evidence for graphenelike two-dimensional silicon, *Phys. Rev. Lett.* 108 (2012) 155501.
- [4] M.E. Davila, L. Xian, S. Cahangirov, A. Rubio, G. Le Lay, Germanene: a novel two-dimensional germanium allotrope akin to graphene and silicene, *New J. Phys.* 16 (2014) 3579–3587.
- [5] H. Liu, A.T. Neal, Z. Zhu, Z. Luo, X. Xu, D. Tomanek, P.D. Ye, Phosphorene: an unexplored 2D semiconductor with a high hole mobility, *ACS Nano* 8 (2014) 4033–4041.
- [6] J.H. Lee, Gas sensors using hierarchical and hollow oxide nanostructures: overview, *Sensor. Actuat. B - Chem.* 140 (2009) 319–336.
- [7] F. Xu, W. Yu, R. Gao, Q. Zhou, Q. Zhang, W. Wang, Dioxin formations from the radical/radical cross-condensation of phenoxy radicals with 2-chlorophenoxy radicals and 2,4,6-trichlorophenoxy radicals, *Environ. Sci. Technol.* 44 (2010) 6745–6751.
- [8] J. Dai, P. Giannozzi, J. Yuan, Gas adsorption on graphene doped with B, N, Al, and S: a theoretical study, *Appl. Phys. Lett.* 95 (2009) 183.
- [9] I. Lopez-Corral, S. Piriz, R. Faccio, A. Juan, M. Avena, A van der Waals DFT study of PtH<sub>2</sub> systems absorbed on pristine and defective graphene, *Appl. Surf. Sci.* 382 (2016) 80–87.
- [10] I. Lopez-Corral, E. German, A. Juan, M.A. Volpe, G.P. Brizuela, Hydrogen adsorption on palladium dimer decorated graphene: a bonding study, *Int. J. Hydrogen Energy* 37 (2012) 6653–6665.
- [11] Z. Qian, M.S.L. Hudson, H. Raghunathi, R.H. Scheicher, B. Pathak, C.M. Araujo, A. Blomqvist, B. Johansson, O.N. Srivastava, R. Ahuja, Excellent catalytic effects of graphene nanofibers on hydrogen release of sodium alanate, *J. Phys. Chem. C* 116 (2012) 10861–10866.
- [12] W. Yuan, G. Shi, Graphene-based gas sensors, *J. Mater. Chem. A* 1 (2013) 10078–10091.
- [13] B. Cho, J. Yoon, M.G. Hahm, D.-H. Kim, A.R. Kim, Y.H. Kahng, S.W. Park, Y.J. Lee, S.G. Park, J.D. Kwon, C.S. Kim, M. Song, Y. Jeong, K.S. Nam, H.C. Ko, Graphene-based gas sensor: metal decoration effect and application to a flexible device, *J. Mater. Chem. C* 2 (2014) 5280–5285.
- [14] J. Prasongkit, R.G. Amorim, S. Chakraborty, R. Ahuja, R.H. Scheicher, V. Amornkitbamrun, Highly Sensitive and selective gas detection based on silicene, *J. Phys. Chem. C* 119 (2015) 16934–16940.
- [15] L. Kou, T. Frauenheim, C. Chen, Phosphorene as a superior gas sensor: selective adsorption and distinct I-V response, *J. Phys. Chem. Lett.* 5 (2014) 2675–2681.
- [16] S. Noorizadeh, E. Shakerzadeh, Formaldehyde adsorption on pristine, Al-doped and mono-vacancy defected boron nitride nanosheets: a first principles study, *Comput. Mater. Sci.* 56 (2012) 122–130.
- [17] Q. He, Z. Zeng, Z. Yin, H. Li, S. Wu, X. Huang, H. Zhang, Fabrication of flexible MoS<sub>2</sub> thin-film transistor arrays for practical gas-sensing applications, *Small* 8 (2012) 2994–2999.
- [18] C.W. Zhang, First-principles study on electronic structures and magnetic properties of AlN nanosheets and nanoribbons, *J. Appl. Phys.* 111 (2012) 153.
- [19] S. Valedbagi, A. Fathalian, S.M. Elahi, Electronic and optical properties of AlN nanosheet: an ab initio study, *Opt. Commun.* 309 (2013) 153–157.
- [20] X. Zhang, Z. Liu, S. Hark, Synthesis and optical characterization of single-crystalline AlN nanosheets, *Solid State Commun.* 143 (2007) 317–320.
- [21] Y. Li, Z. Yang, Z. Chen, Z. Zhou, Computational investigation on structural and physical properties of AlN nanosheets and nanoribbons, *J. Nanosci. Nanotechnol.* 10 (2010) 7200–7203.
- [22] C.W. Zhang, F.B. Zheng, First-principles prediction on electronic and magnetic properties of hydrogenated AlN nanosheets, *J. Comput. Chem.* 32 (2011) 3122–3128.
- [23] C.W. Zhang, P.J. Wang, Tuning electronic and magnetic properties of AlN nanosheets with hydrogen and fluorine: first-principles prediction, *Phys. Lett. A* 375 (2011) 3583–3587.
- [24] M.D. Ganji, S. Jameh-Bozorgi, M. Rezvani, A comparative study of structural and electronic properties of formaldehyde molecule on monolayer honeycomb structures based on vdW-DF prospective, *Appl. Surf. Sci.* 384 (2016) 175–181.
- [25] S.F. Rastegar, N.L. Hadipour, H. Soleymanabadi, Theoretical investigation on the selective detection of SO<sub>2</sub> molecule by AlN nanosheets, *J. Mol. Model.* 20 (2014) 2439.
- [26] S.F. Rastegar, A.A. Peyghan, H.R. Ghenaatian, N.L. Hadipour, NO<sub>2</sub> detection by nanosized AlN sheet in the presence of NH<sub>3</sub>: DFT studies, *Appl. Surf. Sci.* 274 (2013) 217–220.
- [27] T. Ouyang, Z. Qian, R. Ahuja, X. Liu, First-principles investigation of CO adsorption on pristine, C-doped and N-vacancy defected hexagonal AlN nanosheets, *Appl. Surf. Sci.* 439 (2018) 196–201.
- [28] Y.H. Zhang, Y.B. Chen, K.G. Zhou, C.H. Liu, J. Zeng, H.L. Zhang, Y. Peng, Improving gas sensing properties of graphene by introducing dopants and defects: a first-principles study, *Nanotechnology* 20 (2009) 185504.
- [29] T. Hussain, T. Kaewmaraya, S. Chakraborty, R. Ahuja, Defect and substitution-induced silicene sensor to probe toxic gases, *J. Phys. Chem. C* 120 (2016) 25256–25262.
- [30] M.S. Mahabal, M.D. Deshpande, T. Hussain, R. Ahuja, Sensing characteristics of phosphorene monolayers toward PH<sub>3</sub> and AsH<sub>3</sub> gases upon the introduction of vacancy defects, *J. Phys. Chem. C* 210 (2016) 20428–20436.
- [31] D. Ma, Q. Wang, T. Li, C. He, B. Ma, Y. Tang, Z. Lu, Z. Yang, Repairing sulfur

- vacancies in the MoS<sub>2</sub> monolayer by using CO, NO and NO<sub>2</sub> molecules, *J. Mater. Chem. C* 4 (2016) 7093–7101.
- [32] J.A. Nadel, H. Salem, B. Tamplin, Y. Tokiwa, Mechanism of bronchoconstriction During inhalation of Sulfur Dioxide, *J. Appl. Physiol.* 20 (1965) 164–167.
- [33] X. Liu, K. Sun, Y. Qu, M. Hu, Y. Sun, F. Zhang, Y. Zhang, Secondary formation of sulfate and nitrate during a haze episode in Megacity Beijing, China, *Aerosol Air Qual. Res.* 15 (2015) 2246–2257.
- [34] J.L. Devalia, C. Rusznak, M.J. Herdman, C.J. Trigg, H. Tarraf, R.J. Davies, Effect of nitrogen-dioxide and sulfur-dioxide on airway response of mild asthmatic-patients to allergen inhalation, *Lancet* 344 (1994) 1668–1671.
- [35] G. Kresse, J. Hafner, Ab-initio molecular-dynamics for liquid-metals, *Phys. Rev. B* 47 (1993) 558–561.
- [36] G. Kresse, J. Hafner, Ab-initio molecular-dynamics for open-shell transition-metals, *Phys. Rev. B* 48 (1993) 13115–13118.
- [37] G. Kresse, J. Hafner, Ab-initio molecular-dynamics simulation of the liquid-metal amorphous-semiconductor transition in germanium, *Phys. Rev. B* 49 (1994) 14251–14269.
- [38] G. Kresse, J. Furthmuller, Efficiency of ab-initio total energy calculations for metals and semiconductors using a plane-wave basis set, *Comput. Mater. Sci.* 6 (1996) 15–50.
- [39] G. Kresse, J. Furthmuller, Efficient iterative schemes for ab initio total-energy calculations using a plane-wave basis set, *Phys. Rev. B* 54 (1996) 11169–11186.
- [40] P.E. Blochl, Projector augmented-wave method, *Phys. Rev. B* 50 (1994) 17953–17979.
- [41] J.P. Perdew, K. Burke, M. Ernzerhof, Generalized gradient approximation made simple, *Phys. Rev. Lett.* 77 (1996) 3865–3868.
- [42] S. Grimme, Semiempirical GGA-type density functional constructed with a long-range dispersion correction, *J. Comput. Chem.* 27 (2006) 1787–1799.
- [43] H.J. Monkhorst, J.D. Pack, Special points for brillouin-zone integrations, *Phys. Rev. B* 13 (1976) 5188–5192.
- [44] J. Glosowski, Atoms in molecules – a quantum theory-bader, *RFW, Science* 252 (1991) 1566–1567.
- [45] R. Ahmed, H. Akbarzadeh, A. Fazel e, A first principle study of band structure of III-Nitride Compounds, *Physica B Condens.* 370 (2005) 52–60.